Energy & Environmental Science

Accepted Manuscript

This article can be cited before page numbers have been issued, to do this please use: H. Zhou, H. Duan, W. Yang, Q. Chen, C. Hsu, W. Hsu, C. Chen and Y. Yang, *Energy Environ. Sci.*, 2013, DOI: 10.1039/C3EE43101K.

This is an *Accepted Manuscript*, which has been through the RSC Publishing peer review process and has been accepted for publication.

Accepted Manuscripts are published online shortly after acceptance, which is prior to technical editing, formatting and proof reading. This free service from RSC Publishing allows authors to make their results available to the community, in citable form, before publication of the edited article. This *Accepted Manuscript* will be replaced by the edited and formatted *Advance Article* as soon as this is available.

To cite this manuscript please use its permanent Digital Object Identifier (DOI®), which is identical for all formats of publication.

More information about *Accepted Manuscripts* can be found in the **Information for Authors**.

Please note that technical editing may introduce minor changes to the text and/or graphics contained in the manuscript submitted by the author(s) which may alter content, and that the standard **Terms & Conditions** and the **ethical guidelines** that apply to the journal are still applicable. In no event shall the RSC be held responsible for any errors or omissions in these *Accepted Manuscript* manuscripts or any consequences arising from the use of any information contained in them.

View Article Online
DOI: 10.1039/C3EE43101K

Facile single-component precursor for Cu_2ZnSnS_4 with enhanced phase and composition controllability

*Huanping Zhou[+], Hsin-Sheng Duan[+], Wenbing Yang, Qi Chen, Chia-Jung Hsu, Wan-Ching Hsu, Chun-Chao Chen and Yang Yang**

Dr. H. P. Zhou, H.-S, Duan, Dr. W. B. Yang, Dr. Qi Chen, C.-J. Hsu, W.-C. Hsu, C.-C. Chen, and Prof. Y. Yang

Department of Materials Science and Engineering
University of California Los Angeles, Los Angeles, CA 90095, USA
+These authors contributed equally to this work.
*E-mail: yangy@ucla.edu

Abstract

A simple and effective method has been demonstrated using soluble single-component precursors to achieve high quality Cu_2ZnSnS_4 (CZTS) thin film with enhanced phase and composition controllability. The soluble single-component precursors were composed of $Cu_{2-x}S$ colloidal nanocrystals (NC) and the homogeneously distributed Zn-Sn species on the surface. Zn species is presented as the surface ligand for the first time, in the form of Zn-Sn complex, providing both the colloidal stabilization and the essential components for CZTS. CZTS film composition is governed by the prescribed stoichiometry between $Cu_{2-x}S$ nanoparticles and the Zn-Sn complex in solution. This novel reaction process enables a favorable CZTS phase progression, with less than 175 °C formation temperature, and a minimized secondary phase growth mode, due to its local composition uniformity in both liquid and film state. Compared with the approaches based on molecular precursor or quarternary CZTS nanocrystals, the single-compoent precusor allows fine tune of the kesterite materials for future advanced optoelectronics.

Keywords: single component, Cu_2ZnSnS_4, composition control, phase progression, solar cell

View Article Online
DOI: 10.1039/C3EE43101K

Introduction

Kesterite-phase Cu_2ZnSnS_4 (CZTS) has recently been highlighted as emerging absorber material in next generation thin film solar cells, owing to its decent optical property and earth abundant nature.[1,2] The successful demonstration of CZTS processing,[3–11] is largely benefit from controlling the formation of the kesterite phase, a target that poses unique material challenges. Unlike its analogous $Cu(In,Ga)S_2$ (CIGS) or CdTe,[12–14] single-phase kesterite CZTS exists only within a narrow stoichiometry range.[15,16] The presence of volatile elemental constituents and binary phases[17–19] (such as zinc metal and tin chalcogenide) further complex the phase purity issue within the deposited films, particularly under high temperatures and vacuum conditions. Thus, the exquisite controllability over composition[20–24] and phase becomes the key prerequisite in any synthetic routes for the fabrication of high performance CZTS films.

Similar with other members of metal chalcogenide family, high quality CZTS films have been deposited *via* a cost-effective solution processing.[3,5] Solution processing, by taking advantages of its high precursor diffusivity and uniform precursor distribution in liquids, is capable of producing pure kesterite phase at low temperature.[4,5,19] An ideal solution precursor for high quality kesterite phase requires identical compositions in both liquid and film, absence of impurities, precise control on composition stoichiometry, free of phase segregation and small geometry reorganization during film formation. Despite the remarkable progresses, current solution processing precursors, varying from solution mixture of multiple molecules or binary/ternary nanoparticles, quarternary particles to preformed single-component quaternary nanoparticles, still hardly meet all the criteria.[7–9] Solution mixture of multiple molecular or binary/ternary nanoparticles enables large stoichiometry tunablility, however, the local element distribution in spin-coated films is uncertain owing to phase segregation, which may lead to an intensive kinetically ion diffusion barrier during phase formation. A single-component precursor,

View Article Online
DOI: 10.1039/C3EE43101K

such as quaternary kesterite-phase CZTS nanocrystals with only one composition, enables identical local compositions in both liquid and film state, but on the cost of surface long chain hydrocarbon ligands contaminating film purity. Thus, developing a clean uniform solution precursor that exhibits controllability over composition and phase progression during film formation is highly preferable.

We report, for the first time, a facile single-component nanoparticle precursor, $Cu_{2-x}S$ nanoparticles (NPs) capped with Zn-Sn complex (Zn-Sn complex abbreviates the mixture of $Zn(hyc)_2(N_2H_4)_2$ (hyc: hydrazinocarboxylic), $[Sn_2S_7]^{6-}$ and $[SnS_4]^{4-}$), for high-quality kesterite-phase CZTS film (Scheme 1). In this approach, Zn-Sn complex is directly capped onto the ultra-small $Cu_{2-x}S$ nanoparticles surface to form homogeneous nanoparticles. Compared with quaternary kesterite-phase CZTS nanocrystals, $Cu_{2-x}S$/Zn-Sn nanoparticle ($Cu_{2-x}S$/Zn-Sn) precursor exhibits similar composition controllability, resulted from their single-component nature, but the absence of surface hydrocarbon ligands. Upon annealing, local element re-distribution produces the resulting kesterite-phase CZTS with increased film homogeneity and less impurities. Surface Zn-Sn ligands surrounding $Cu_{2-x}S$ nanoparticles provide both colloidal stabilization and essential components for CZTS. The stoichiometry of CZTS is simply adjusted by the concentration of $Cu_{2-x}S$ nanoparticles and Zn-Sn ligands. Film formation is investigated in detail with X-ray diffraction and Raman spectroscopy. We find that, with current single-component nanoparticle precursor, very few steps are required to produce kesterite Cu_2ZnSnS_4 phase. Using the present precursor, photovoltaic devices have been successfully demonstrated, and advanced optoelectronics are expected by precisely tuning the kesterite material properties.

Experimental

Chemicals: All chemicals are purchased from Aldrich, and used without any further purification.

View Article Online
DOI: 10.1039/C3EE43101K

Synthesis of $Cu_{2-x}S$ nanoparticles: The synthesis of $Cu_{2-x}S$ nanoparticles followed the literature method.[25] In a typical synthesis, 1.25 mmol of ammonium diethyldithiocarbamate is mixed with 10 mL of dodecanethiol and 17 mL of oleic acid in a three-neck flask. Then, the solution is heated up to 110 °C under Argon (Ar) flow and maintained at 110 °C for 30 minutes, followed by a quick injection of a suspension composed of 1 mmol of copper(II) acetylacetonate and 3 mL of oleic acid. After that, the solution is quickly heated up to 180 °C and kept at the temperature for 10 minutes. The solution containing $Cu_{2-x}S$ nanoparticles is cooled down naturally to room temperature before was taken out of the flask for centrifuging at 5000 rpm for 8 minutes. The supernatant is discarded and the precipitation is first fully dissolved in 4 mL of toluene and then precipitated out by adding 30 mL of isopropanol followed by centrifuging at 5000 rpm for 8 minutes. The as-obtained precipitation is fully dissolved in toluene with mass concentration of 20 mg/mL $Cu_{2-x}S$ nanoparticles for further construction of CZTS precursor.

Preparation of Zn-Sn ligand solution: The Zn-Sn hydrazine solution was prepared according to the previous work of our group.[26] In brief, Zinc nanopowder (2 mmol) was mixed and stirred with $H_2NNHCOOH$ saturated hydrazine solution (1 mL), which was first prepared by adding hydrazine to a vial containing solid-state carbon dioxide. The tin precursor solution was prepared in a separate vessel, through mixing SnS_2 (1 mmol) and excess sulfur (2 mmol) in N_2H_4 (1 mL) with stirring. The Zn-Sn hydrazine solution was made by mixing the above two solution with adjusted molar ratio of Zn/Sn = 1.2. Note: Hydrazine is highly toxic, and appropriate protective equipment should be used to prevent direct contact with the liquid or vapor. The reaction between carbon dioxide and hydrazine is highly exothermic. The hydrazine-based solutions were prepared in a nitrogen-filled glove box where the oxygen and moisture levels were both below 1 ppm. The Zn-Sn dried precursor was prepared by evaporating Zn-Sn hydrazine solution

View Article Online
DOI: 10.1039/C3EE43101K

overnight, and was re-dissolved in appropriate amount of benign solvents, such as formamide (FA), ethanolamine (EA) with continuous stirring at 100 °C for 1-2 h. The as-prepared Zn-Sn species in EA or FA are adjusted with desired concentration for the construction of CZTS precursor solution in the next step.

Preparation of CZTS precursor: The final CZTS precursor solution was prepared by mixing the following constituents, 0.3 mL 0.2 M Zn-Sn solution of FA, 0.5 mL 20mg/mL $Cu_{2-x}S$ colloidal solution of toluene and 0.2 mL extra FA in the glovebox. The as-formed two-phase mixture was stirred vigorously for several hours, after which toluene phase turned colorless while the FA phase turned black, indicating ligand exchange of nanocrystals. The colorless upper toluene phase was discarded and the bottom FA phase was washed three times with toluene. Then, the bottom black layer was collected by adding adequate amount of acetonitrile, followed by centrifuging at 5000 rpm for 6 min, and lastly was re-dispersed in FA solvent. The as-obtained CZTS precursor solution was stored in the glovebox for further characterization and device fabrication. For FTIR characterization, the precursor solution is dried under vacuum in order to measure its solid state behaviour. The off-stoichiometric CZTS precursor solution was prepared by mixing excessive Zn-Sn solution with $Cu_{2-x}S$ nanocrystals, e.g. 0.4 mL 0.2 M Zn-Sn solution and 0.5 mL 20 mg/mL $Cu_{2-x}S$ colloidal solution, and the rest of the preparation procedures remain the same.

Fabrication and characterization of $Cu_2ZnSn(S,Se)_4$ (CZTSSe) solar cells: CZTSSe absorber was deposited onto the molybdenum-coated glass substrate by spin-coating the precursor solution multiple times, with intermediate annealing steps of 300 °C followed by a final selenization in a graphite box at 560 °C for 20 minutes. The cadmium sulfide (CdS) layer was then deposited onto CZTSSe layer by chemical bath deposition. Finally, Ag nanowires

View Article Online
DOI: 10.1039/C3EE43101K

(NW)/ITO-nanoparticles films were spin coated onto the devices as a transparent top electrode. The area of each cell was 2 mm by 2.5 mm, defined by mechanical scribing of a 1 cm by 1 cm substrate. The current versus voltage (J-V) performance was measured under an AM 1.5G filter at 100 mW/cm^2, using a Newport Oriel 92192 solar simulator.

Materials Characterization: Both the films and powder samples were annealed at the desired temperature on a hot plate with the temperature verified by an IR thermometer. XRD patterns were collected on a PANalytical X'Pert Pro X-ray powder diffractometer using Cu Kα radiation (λ=1.54060 Å). The scanning electron microscope (SEM) images were taken on Nova 230 with an accelerating voltage of 5 kV. Raman shift spectroscopy was carried out using a Renishaw inVia Raman microscope using an excitation laser with a wavelength of 514 nm. TEM images were taken on an FEI CM120 microscope operating at 120 kV, and FEI Titan 80-300 kV S/TEM operating at 300 KV. FTIR spectra were obtained on a PerkinElmer Paragon 1000 FT-IR Spectrometer at a resolution of 4 cm^{-1} with a PerkinElmer IR microscope.

Results and Discussion

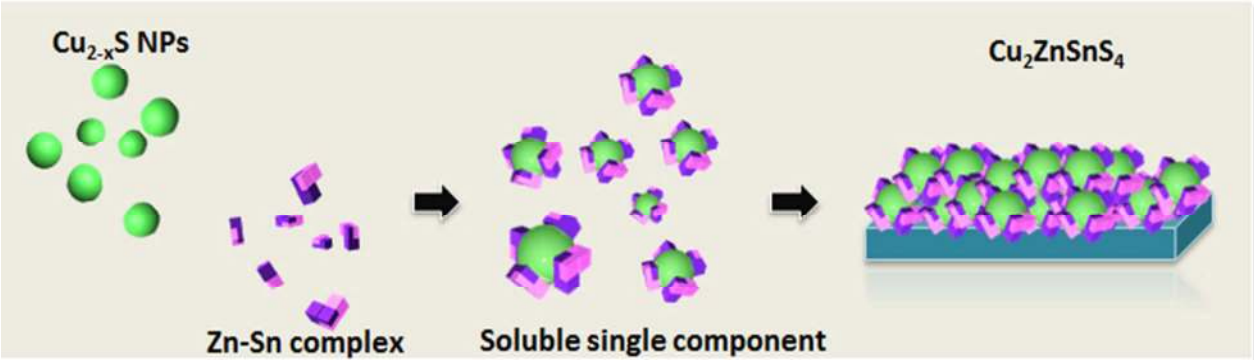

Scheme 1. A schematic illustration of the synthetic route to CZTS film. Initially, $Cu_{2-x}S$ nanoparticles were capped with Zn-Sn complexes to form the single-component precursor, $Cu_{2-x}S$/Zn-Sn nanoparticles. Then $Cu_{2-x}S$/Zn-Sn nanoparticles were deposited into the precursor film, followed by thermal annealing to form the kesterite CZTS film.

View Article Online
DOI: 10.1039/C3EE43101K

The single-component precursor, $Cu_{2-x}S$/Zn-Sn, was synthesized by a two-step ligand-exchange reaction, as illustrated in Figure 1. In brief, $Cu_{2-x}S$ nanoparticles were firstly synthesized, followed by a surface ligand exchange from oleic acid to Zn-Sn ligands. $Cu_{2-x}S$ nanoparticles were firstly synthesized following a literature method,[25,27] where copper acetylacetonate and ammonium diethyldithiocarbamate reacted in a mixed solvent of dodecanethiol and oleic acid. Figure 1a and inset show the Transmission Electron Microscopy (TEM) and High Resolution Transmission Electron Microscopy (HRTEM) images of the as-obtained $Cu_{2-x}S$ nanoparticles. The average size of the nanoparticles was measured as 5.2 ± 0.4 nm, based on TEM statistic results. Characteristic interplanar distance of 0.2 nm from the (110) planes of single-crystal hexagonal $Cu_{2-x}S$ was also observed in the HRTEM image (inset of Figure 1a). X-ray Diffraction (XRD) further confirmed the hexagonal chalcocite $Cu_{2-x}S$ (JCPDS 012-0176, Figure S1, Supporting Information) phase of the as-prepared $Cu_{2-x}S$ nanoparticles, which was in agreement with the TEM results.

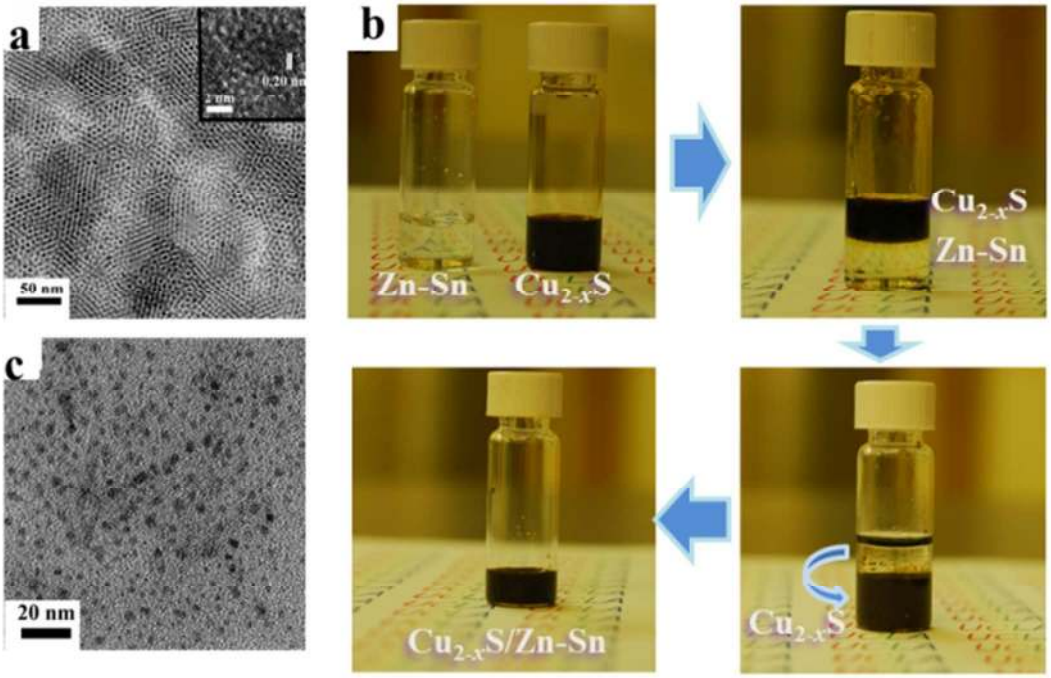

View Article Online
DOI: 10.1039/C3EE43101K

Figure 1 (a) TEM images of the as-prepared oleic acid capped $Cu_{2-x}S$ nanoparticles; (b) Photograph of $Cu_{2-x}S$ nanoparticles before and after ligand exchange of Zn-Sn ligand; (c) TEM images of Zn-Sn ligand capped $Cu_{2-x}S$ nanoparticles.

The Zn-Sn ligand solution was separately prepared by evaporating Zn-Sn hydrazine solution (including $Zn(hyc)_2(N_2H_4)_2$ (hyc: hydrazinocarboxylic), $[Sn_2S_7]^{6-}$, and $[SnS_4]^{4-}$)[26] into a dried precursor, followed by re-dissolution into formamide (FA).[28] Upon the mixing with $Cu_{2-x}S$ nanoparticles solution, Zn and Sn constituents substituted the original surface oleic acid ligands. Figure 1b showed the sequential images before and after ligand exchange. Original $Cu_{2-x}S$ nanoparticles in the toluene phase were then transferred into the Zn-Sn containing FA phase, leaving a transparent toluene layer on the top. Stable $Cu_{2-x}S$/Zn-Sn precursors were finally harvested by centrifuging and re-dispersing the bottom layer. TEM image showed similar morphology of $Cu_{2-x}S$ before (Figure 1a) and after (Figure 1c) surface ligand exchange. Notably, only capped nanoparticles were stabilized in FA, preserving the surface modification uniformity at single particle scale. Also, inadequate amount of Zn-Sn complex ligands versus Cu species would lead to the precipitation of $Cu_{2-x}S$ nanoparticles in formamide. Thus, successfully preparing the CZTS precursor solution in formamide without precipitate indicates the presence of single-component nanoparticles, rather than simply the mixture of $Cu_{2-x}S$ nanoparticles and Zn-Sn complex ligands, in the CZTS precursor solution. In addition, to prove the homogenous distribution of Zn-Sn complex on $Cu_{2-x}S$ nanoparticles, a scanning transmission electron microscopy (STEM)-energy dispersive spectrum (EDS) measurement was conducted (Figure 2). Because of the weak signal from a single nanoparticle (size of ~5 nm), a scanning range of ~45 nm (the inset of Figure 2a) that covered several nanoparticles, was selected as our measurement scope. The plots of metal composition at varied scanning positions were drawn for Cu, Zn and

View Article Online
DOI: 10.1039/C3EE43101K

Sn, respectively (Figure 2b). The signals of Cu, Zn and Sn follow similar distribution profiles, indicating that the Zn-Sn complexes ligands likely capped on the surface of $Cu_{2-x}S$ nanoparticles evenly.

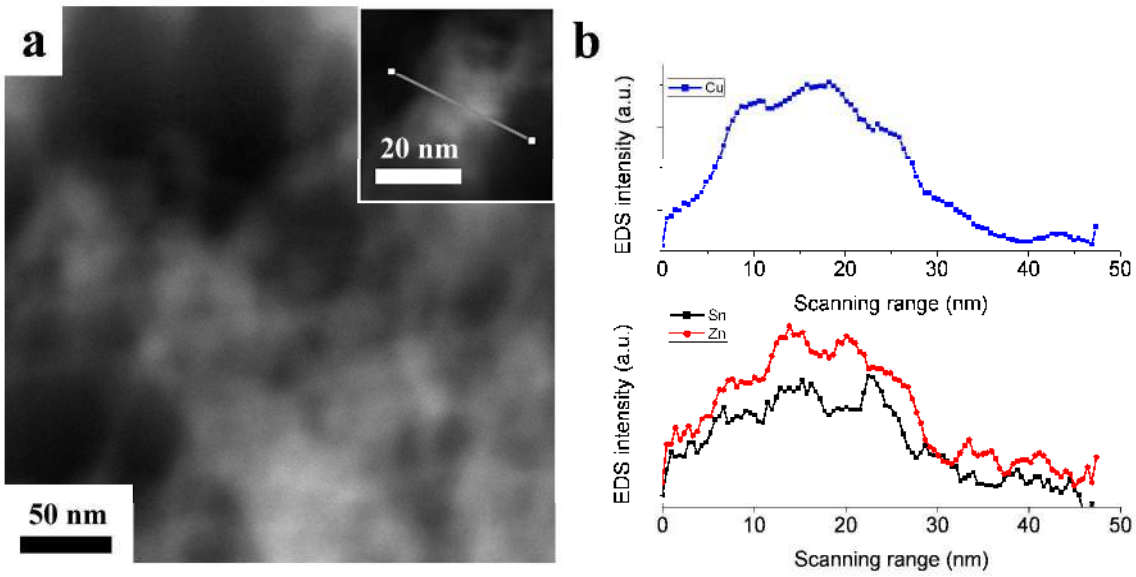

Figure 2: (a) a STEM image of $Cu_{2-x}S$ nanoparticles capped with Zn-Sn complexes; (b) a EDS line scan of the several $Cu_{2-x}S$ nanoparticles capped with Zn-Sn complexes shown in the inset of figure (a), showing the distribution of Cu (top), Zn and Sn (bottom), respectively.

The successful fabrication of single-component $Cu_{2-x}S$/Zn-Sn nanoparticle precursor was further confirmed by FTIR and Raman spectra. As shown in Figure 3a, solid-state FTIR studies indicated the removal of the original hydrocarbon ligands: the characteristic C–H vibrations peak at 2800–3000 cm^{-1} disappeared after the ligand exchange. In Raman spectra (Figure 3b), after ligand exchange, the peak around 300 cm^{-1} and 352 cm^{-1}, indicative of the bridge vibration of $S_3Sn–S–SnS_3$ and $[SnS_4]^{4-}$ stretching mode, disappeared, while two new peaks at 334 cm^{-1} and 475 cm^{-1} likely from Cu_2ZnSnS_4 and Cu_2S were observed, respectively.[19,29,30] Importantly, the appearance of Cu_2ZnSnS_4 vibration at 334 cm^{-1} indicates the surface binding between $Cu_{2-x}S$

View Article Online
DOI: 10.1039/C3EE43101K

nanoparticles and Zn and Sn species at room temperature, and the effective surface distribution of Zn and Sn around $Cu_{2-x}S$ nanoparticles.

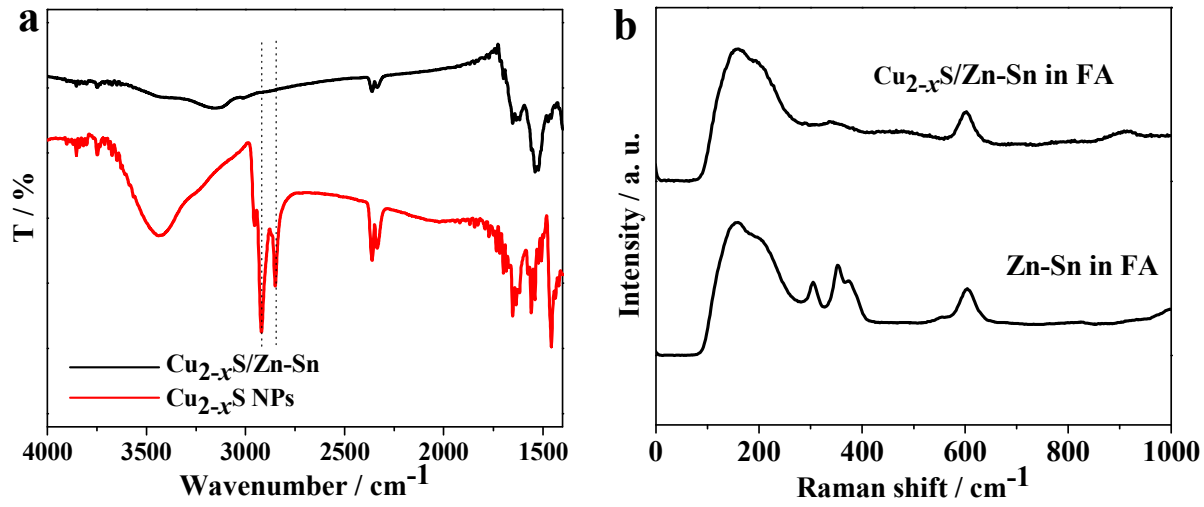

Figure 3: (a) FTIR spectra of the $Cu_{2-x}S$ nanoparticles, before (red line) and after (black line) ligand exchange with Zn-Sn complex; (b) Raman spectra of Zn-Sn precursors in FA and $Cu_{2-x}S$ nanoparticles with Zn-Sn complexes in FA.

Next we investigated the phase formation and intermediate products within the as-deposited film *via* temperature-dependent XRD and Raman spectrum. At each temperature, the film was incubated for 10 minutes, and then characterized by XRD and Raman, as shown in Figure 4. At 100 °C, strong signals from $Cu_{2-x}S$ and amorphous hydrazinium frameworks were recorded in XRD. Due to the spectrum overlap, diffraction patterns from the crystalline phases of CZTS or its sub-phases were hard to be identified. Same sample exhibits one Raman peak at 470 cm^{-1}, in good agreement with the reported vibrational mode of $Cu_{2-x}S$ phase.[31] Besides, there is a broad peak appeared at 330 cm^{-1} with a shoulder at 298 cm^{-1}, suggesting the formation of Cu_2ZnSnS_4 or Cu_2SnS_3.[32]

View Article Online
DOI: 10.1039/C3EE43101K

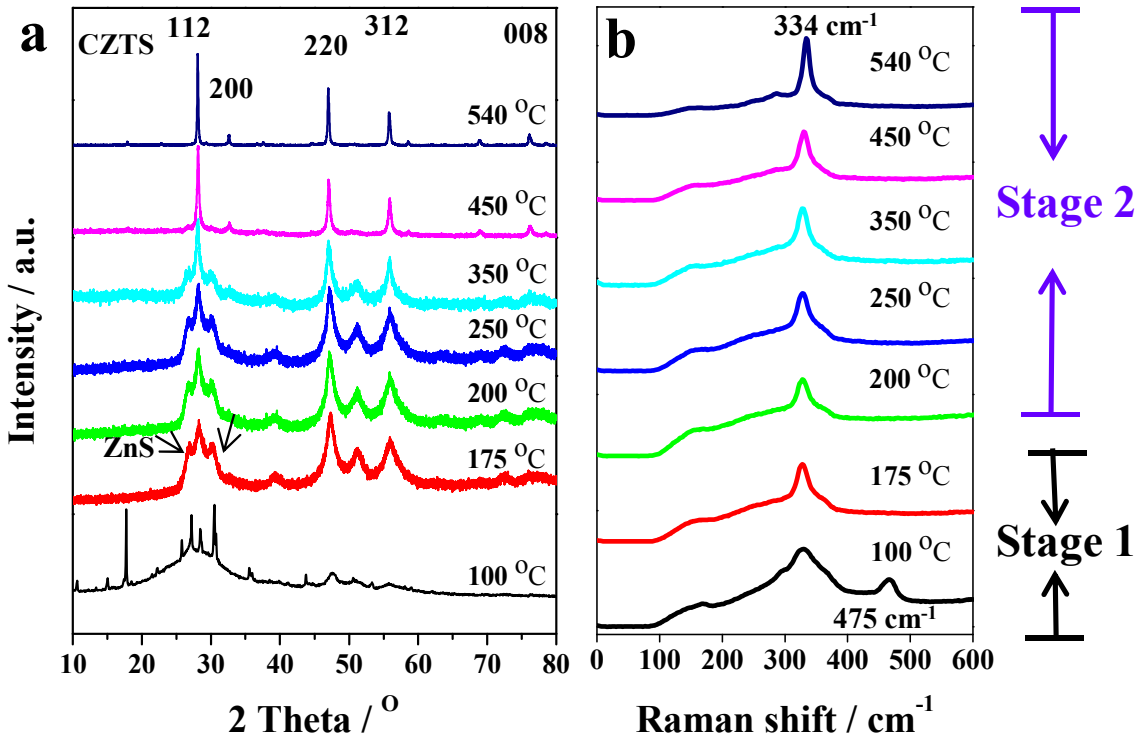

Figure 4: (a) XRD patterns and (b) Raman spectra of $Cu_{2-x}S$ nanocrsytal and Zn-Sn ligand precursor annealed at various temperatures. Stage 1 (RT–175 °C): formation Cu_2ZnSnS_4 or Cu_2SnS_3 based on reaction between $Cu_{2-x}S$ and Zn-Sn species; stage 2 (175 °C–540 °C): formation of pure kesterite Cu_2ZnSnS_4 from Cu_2SnS_3 and ZnS.

When the temperature reached 175 °C (stage 1), we observed clear signs indicative of dramatic phase changes from $Cu_{2-x}S$ to Cu_2ZnSnS_4 or Cu_2SnS_3. XRD diffraction from $Cu_{2-x}S$ disappeared, together with the appearance of a mixture of diffraction patterns from hexagonal phase of ZnS (JCPDS 00-005-0492) and a cubic phase, from either Cu_2SnS_3 (JCPDS 01-089-2879) or Cu_2ZnSnS_4 (JCPDS 00-026-0575), appeared in XRD spectrum. The appearance of these bimetallic or trimetallic chalcogenides, clearly indicated the reaction between $Cu_{2-x}S$ nanoparticles and Zn-Sn ligands at mild conditions, even though it is challenging to differentiate

View Article Online
DOI: 10.1039/C3EE43101K

the close phases of Cu_2SnS_3 and Cu_2ZnSnS_4. Same phase change was also evidenced in Raman spectrum, where a strong peak at 330 cm^{-1} from the dominant phase of Cu_2ZnSnS_4 or Cu_2SnS_3 appeared instead of the Cu_2S peak. Notably, we didn't observe the wurtzite ZnS in Raman spectrum owing to the lack of proper laser source to excite the corresponding vibrations. The new formed phases appeared around $Cu_{2-x}S$ nanoparticles, suggesting the single-component precursor as the nucleation center for the phase formation in the film.

Further temperature increment kept triggering phase change till the complete formation of kesterite Cu_2ZnSnS_4 (stage 2). From 200 °C to 540 °C, the characteristic diffraction patterns from wurtzite ZnS, gradually decreased till final diminish; whereas diffraction intensity from crystallined kesterite Cu_2ZnSnS_4 on the contrary, was increasing, till all its characteristic peaks appearing, evidencing a pure kesterite Cu_2ZnSnS_4 in the film. In Raman, the improvement crystallined kesterite Cu_2ZnSnS_4 promoted the peak intensity at around 330 cm^{-1} during the whole stage 2.

The complementary study based on XRD and Raman spectroscopy suggested a two-stage film formation upon annealing. Starting from the single-component precursor, $Cu_{2-x}S$/Zn-Sn nanocrystals, $Cu_{2-x}S$ firstly reacts with surface Zn-Sn species to form CZTS or Cu_2SnS_3 at 175 °C (stage 1), which then gradually grows larger till final conversion to the dominant pure kesterite Cu_2ZnSnS_4 stable up to at least 540 °C (stage 2). This two-stage growth is unique compared to other deposition processes starting from pure elements or binary chalcogenides, because the $Cu_{2-x}S$ nanoparticles provide not only key constituent but also nucleation centers for film growth. A homogeneous elemental distribution down to the nanoscale, as indicated in Figure 2, enables a uniform film (Table S1) from the single component precursor. Local ion diffusion within short distances of each precursor may provide a desired phase composition; in

View Article Online
DOI: 10.1039/C3EE43101K

constrast, long-distance ion diffusion is often required in other deposition processes. Similar growth processes have also been reported in hydrazine based approach which starts with $Cu_2Sn(Se,S)_3$ and $Zn(Se,S)N_2H_4$, where much larger nanoparticle mixture are used.[19]

For the first time, $Cu_{2-x}S$ nanocrystals are capped with Zn-Sn complex to form the single-component nanoparticle precursor, $Cu_{2-x}S$/Zn-Sn, towards high-quality uniform kesterite CZTS films. This strategy enables quantitative, facile, and clean CZTS film controllability on both composition and phase formation. For the composition controllability, the element stoichiometry in the as-deposited film is identical to the stoichiometry of $Cu_{2-x}S$ nanoparticles and Zn-Sn complex in solution. Prescribed composition of the film can be directly synthesized by controlling solution concentration and the amount. Preparing the single-component nanoparticle precursor is achieved by direct mixing of multiple constituents at room temperature, without the need to consider incorporation discrimination of multiple elements into nanoparticle or as-deposited film. Phase segregation in molecular solution-deposited or multiple nanoparticle solution is absent with current single-component precursor, ensuring the uniform element distribution, both locally near nucleation centers and globally through the film. For the stoichiometry product fabricated with single-component precursor, no extra XRD patterns, coming from possible secondary phases, such as ZnS in slightly off-stoichiometric composition are observed, as shown in Figure 5a. Substituting hydrocarbon molecules with Zn-Sn complex further ensures only the desired constituents present in the film, and diminishes the carbon contamination that is observed in traditional nanoparticle precursors as shown in Figure 5b.

View Article Online
DOI: 10.1039/C3EE43101K

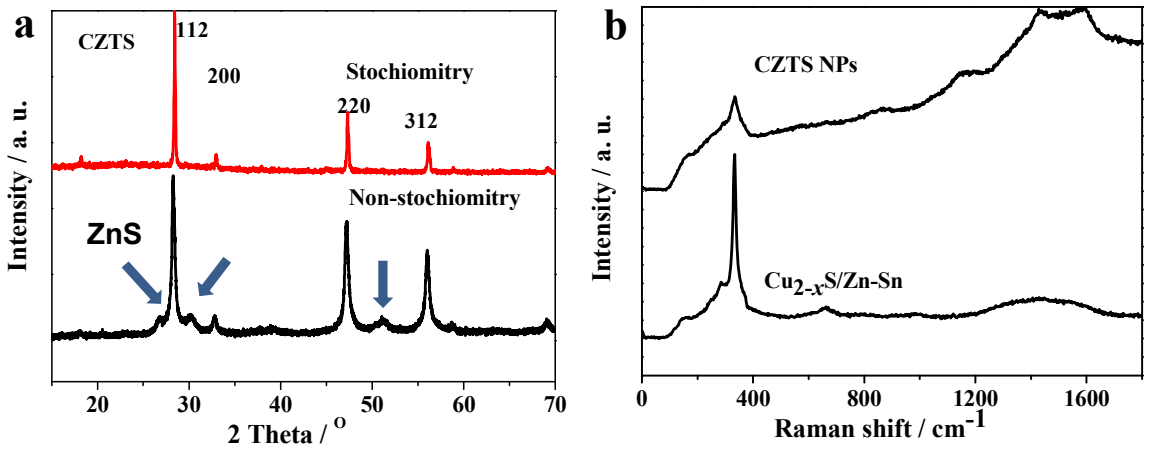

Figure 5: (a) The XRD pattern of the $Cu_{2-x}S$/Zn-Sn precursor solution based film, with adjusted ratio between $Cu_{2-x}S$ nanoparticles and Zn-Sn species; (b) The Raman spectra of $Cu_{2-x}S$/Zn-Sn precursor solution and CZTS nanocrystals. The CZTS nanocrystals was obtained by the procedure detailed in supporting information.

The as-prepared single component CZTS precursors are further used to fabricate the solar cell devices. Figure 6a shows a cross section SEM image of a CZTSSe film after selenization and Figure 6b represents a typical J-V charactestics of a solar cell made from the present CZTS presursor. It is worth nothing that there is an absence of carbon-rich layer in the selenized films, which is different from that based on CZTS nanoparticles capped with long chain carbon ligands. This indicates the successful ligand exchange process, leading to negligible hydrocarbon residues in the final film. In a first optimization, the device exhibits an open circuit voltage (V_{OC}) of 0.151 V, short circuit current (J_{SC}) of 25.3 $mAcm^{-2}$, fill factor (FF) of 30.8%, and power conversion efficiency of 1.2%. Continued optimization of absorber fabrication and interface engineering is underway.

View Article Online
DOI: 10.1039/C3EE43101K

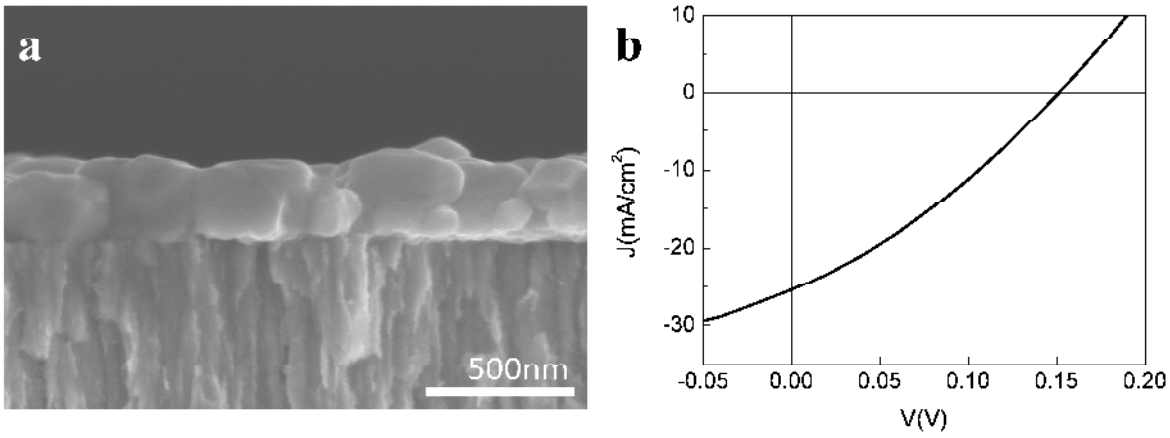

Figure 6: (a) Cross section SEM image of a CZTSSe film after selenization and (b) J-V characteristics of a photovoltaic device prepared from the single-compenent CZTS precursor.

$Cu_{2-x}S$ as the nucleation center might overcome the activation energy barrier of film growth to the thermodynamically stable phase, where the stability of secondary impurity phase is largely decreased. Zn-Sn species are homogeneously distributed on Cu species, producing comparative shorter local diffusion length for all the constituents to reach the thermodynamically equilibrium positions than that in a phase-segregated film. Different from the single-component precursor present here, an alternative approach using $Sn_2Se_6^{4-}$ capped Cu_2Se and ZnS nanocrystals,[33] still needs complex accurate balancing on both composition and ion diffusion among all the constituents. During film formation, significant longer ion diffusion through Sn species separated Cu and Zn nanoparticles are also observed. Hence, pre-formed small nanocrystals serve as perfect models for investigating the mediation of nucleation and growth within a solid-state film from soluble precursors. A more controllable nucleation and growth mode from liquid state to solid state will in turn benefit the development of solid state chemistry.

View Article Online
DOI: 10.1039/C3EE43101K

Using Zn-Sn species as the capping ligands of the colloidal nanocrystals enriches the inorganic ligand family, from single halogen anion or single metal-based metal chalcogenide complex (MCC) to multi-metal-based MCC ligands.[33–36] We have noticed, the presence of multi-metal-based MCC ligands, with their high affinity to replace typical organic ligands on nanoparticle surface, solves both carbon contamination and surface surfactant barrier for ion diffusion. In particular, some inorganic species may perform as the indispensable components to improve performance of designed optoelectronic device, while Zn-Sn species as an inorganic ligand, is a promising candidate with the capability for tuning optical and electrical properties for optoelectronics development.

Conclusion

In summary, we report a facile, quantitative and clean fabrication of kesterite CZTS film from a single-component precursor, crystalline $Cu_{2-x}S$ capped with multi-metal MCC ligands, Zn-Sn complex, and demonstrate its optoelectronic performance. This facile approach possesses unique controllability over CZTS composition and phase formation progression. For the first time, Zn, together with Sn chacolgenide in the form of Zn-Sn complex, are used as surface capping ligand for $Cu_{2-x}S$ to provide both colloidal stability and essential components for CZTS. Kesterite CZTS film composition is thus governed by the prescribed stoichiometry between $Cu_{2-x}S$ nanoparticles and the Zn-Sn complex in solution. The characteristic that Zn-Sn species homogeneously distributed on $Cu_{2-x}S$ nanoparticles, enables a favorable CZTS phase formation pathway, with less than 175 °C formation temperature, and a minimized secondary phase growth mode. Substitution of traditional hydrocarbon capping ligands by Zn-Sn complex significantly decreases the carbon contamination in films, and photovoltaics devices have been successfully

View Article Online
DOI: 10.1039/C3EE43101K

demonstrated. Current strategy, owing to its relative simple processes, clean composition against organic sacrificial groups during annealing, and low-temperature fabrication, could be further expanded to other I-II-IV-VI_4, I-V-VI_2 based electronic and optoelectronic materials. Facile processing of high-quality clean kesterite film will thus contribute to the ongoing development of optoelectronic devices into industry production of next-generation optoelectronics. The combination of pre-formed small nanocrystals and capped essential component serve as perfect models for investigating the mediation of nucleation and growth within a solid-state film from soluble precursors, which will in turn benefit the development of solid state chemistry.

Acknowledgements

This work was financially supported by a grant from the National Science Foundation (grant number: ECCS-1202231, and Program Director: Dr. George N. Maracas).

References

1. D. B. Mitzi, O. Gunawan, T. K. Todorov, K. Wang, and S. Guha, *Sol. Energy Mater. Sol. Cells*, 2011, **95**, 1421–1436.

2. I. L. Repins, M. J. Romero, J. V. Li, S.-H. Wei, D. Kuciauskas, C.-S. Jiang, C. Beall, C. DeHart, J. Mann, W.-C. Hsu, G. Teeter, A. Goodrich, and R. Noufi, *IEEE J. Photovoltaics*, 2012, 1–7.

3. T. K. Todorov, J. Tang, S. Bag, O. Gunawan, T. Gokmen, Y. Zhu, and D. B. Mitzi, *Adv. Energy Mater.*, 2013, **3**, 34–38.

4. T. K. Todorov, K. B. Reuter, and D. B. Mitzi, *Adv. Mater.*, 2010, **22**, E156–9.

5. W. Yang, H.-S. Duan, B. Bob, H. Zhou, B. Lei, C. Chung, S. Li, W. W. Hou, and Y. Yang, *Adv. Mater.*, 2012, **24**, 6323–6329.

6. I. Repins, C. Beall, N. Vora, C. DeHart, D. Kuciauskas, P. Dippo, B. To, J. Mann, W.-C. Hsu, A. Goodrich, and R. Noufi, *Sol. Energy Mater. Sol. Cells*, 2012, **101**, 154–159.

View Article Online
DOI: 10.1039/C3EE43101K

7. Y. Cao, M. S. Denny, J. V Caspar, W. E. Farneth, Q. Guo, A. S. Ionkin, L. K. Johnson, M. Lu, I. Malajovich, D. Radu, H. D. Rosenfeld, K. R. Choudhury, and W. Wu, *J. Am. Chem. Soc.*, 2012, **134**, 15644–7.

8. Q. Guo, H. W. Hillhouse, and R. Agrawal, *J. Am. Chem. Soc.*, 2009, **131**, 11672–3.

9. H. Zhou, W.-C. Hsu, H.-S. Duan, B. Bob, W. Yang, T. Song, C.-J. Hsu, and Y. Yang, *Energy Environ. Sci.*, 2013, **6**, 2822–2838.

10. H.-S. Duan, W. Yang, B. Bob, C.-J. Hsu, B. Lei, and Y. Yang, *Adv. Funct. Mater.*, 2013, **23**, 1466–1471.

11. H. Zhou, T.-B. Song, W.-C. Hsu, S. Luo, S. Ye, H.-S. Duan, C.-J. Hsu, W. Yang, and Y. Yang, *J. Am. Chem. Soc.*, 2013, **135**, 15998–16001.

12. J. J. Chavez, D. K. Ward, B. M. Wong, F. P. Doty, J. L. Cruz-Campa, G. N. Nielson, V. P. Gupta, D. Zubia, J. McClure, and X. W. Zhou, *Phys. Rev. B*, 2012, **85**, 245316.

13. X. W. Zhou, D. K. Ward, B. M. Wong, F. P. Doty, J. A. Zimmerman, G. N. Nielson, J. L. Cruz-Campa, V. P. Gupta, J. E. Granata, J. J. Chavez, and D. Zubia, *Phys. Rev. B*, 2012, **85**, 245302.

14. X. W. Zhou, D. K. Ward, B. M. Wong, and F. P. Doty, *Phys. Rev. Lett.*, 2012, **108**, 245503.

15. A. Nagoya, R. Asahi, R. Wahl, and G. Kresse, *Phys. Rev. B*, 2010, **81**, 113202.

16. S. Schorr, A. Weber, V. Honkimäki, and H.-W. Schock, *Thin Solid Films*, 2009, **517**, 2461–2464.

17. A. Redinger, D. M. Berg, P. J. Dale, and S. Siebentritt, *J. Am. Chem. Soc.*, 2011, **133**, 3320–3.

18. A. Weber, R. Mainz, and H. W. Schock, *J. Appl. Phys.*, 2010, **107**, 013516.

19. W.-C. Hsu, B. Bob, W. Yang, C.-H. Chung, and Y. Yang, *Energy Environ. Sci.*, 2012, **5**, 8564–8571.

20. H. Katagiri, K. Jimbo, M. Tahara, H. Araki, and K. Oishi, *Mater. Res. Soc. Symp. Proc.*, 2009, **1165**, 125–136.

21. F.-J. Fan, L. Wu, M. Gong, G. Liu, Y.-X. W. Wang, S.-H. Yu, S. Chen, L.-W. Wang, and X.-G. Gong, *ACS Nano*, 2013, **7**, 1454–1463.

22. A. Singh, S. Singh, S. Levcenko, T. Unold, F. Laffir, and K. M. Ryan, *Angew. Chem. Int. Ed. Engl.*, 2013.

View Article Online
DOI: 10.1039/C3EE43101K

23. S. Chen, A. Walsh, J.-H. Yang, X. Gong, L. Sun, P.-X. Yang, J.-H. Chu, and S.-H. Wei, *Phys. Rev. B*, 2011, **83**, 1–5.

24. Q. Guo, G. M. Ford, W.-C. Yang, C. J. Hages, H. W. Hillhouse, and R. Agrawal, *Sol. Energy Mater. Sol. Cells*, 2012, **105**, 132–136.

25. Y. Wu, C. Wadia, W. Ma, B. Sadtler, and A. P. Alivisatos, *Nano Lett.*, 2008, **25**, 2–6.

26. W. Yang, H. Duan, K. C. Cha, C. Hsu, W. Hsu, H. Zhou, B. Bob, and Y. Yang, *J. Am. Chem. Soc.*, 2013, **135**, 6915.

27. J. M. Luther, H. Zheng, B. Sadtler, and A. P. Alivisatos, *J. Am. Chem. Soc.*, 2009, **131**, 16851–7.

28. H. Zhou, C.-J. Hsu, W.-C. Hsu, H.-S. Duan, C.-H. Chung, W. Yang, and Y. Yang, *Adv. Energy Mater.*, 2013, **3**, 328–336.

29. J. Campbell, D. P. DiCiommo, H. P. A. Mercier, A. M. Pirani, G. J. Schrobilgen, and M. Willuhn, *Inorg. Chem.*, 1995, **34**, 6265–6272.

30. B. Krebs and W. Schiwy, *Zeitschrift fur Anorg. und Allg. Chemie*, 1973, **398**, 63–71.

31. H. Yoo and J. Kim, *Sol. Energy Mater. Sol. Cells*, 2011, **95**, 239–244.

32. X. Fontané, L. Calvo-Barrio, V. Izquierdo-Roca, E. Saucedo, a. Pérez-Rodriguez, J. R. Morante, D. M. Berg, P. J. Dale, and S. Siebentritt, *Appl. Phys. Lett.*, 2011, **98**, 181905.

33. C. Jiang, J. Lee, and D. V Talapin, *J. Am. Chem. Soc.*, 2012, **134**, 5010–5013.

34. D. B. Mitzi, L. L. Kosbar, C. E. Murray, M. Copel, and A. Afzali, *Nature*, 2004, **428**, 299–303.

35. A. Nag, M. V Kovalenko, J. Lee, W. Liu, B. Spokoyny, and D. V Talapin, *J. Am. Chem. Soc.*, 2011, **133**, 10612–10620.

36. D. V Talapin, J.-S. Lee, M. V Kovalenko, and E. V Shevchenko, *Chem. Rev.*, 2010, **110**, 389–458.

View Article Online
DOI: 10.1039/C3EE43101K

Table of Content

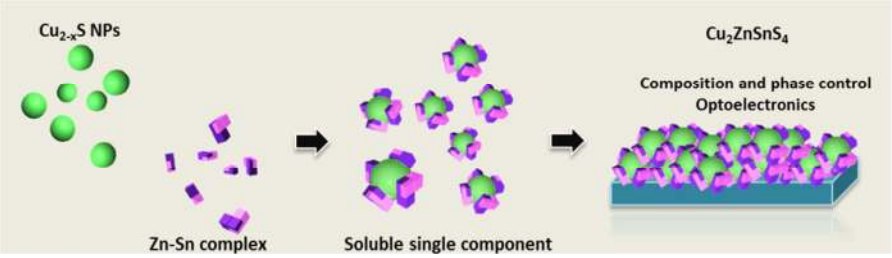

We report a facile, quantitative and clean fabrication of kesterite Cu_2ZnSnS_4 film from a single-component precursor, crystalline $Cu_{2-x}S$ capped with multi-metal metal chacolgenide ligands, Zn-Sn complex, and demonstrate its optoelectronic performance.